


Communication

Wavelength-Tunable L-Band High Repetition Rate Erbium-Doped Fiber Laser Based on Dissipative Four-Wave Mixing

Kai Li, Qianqian Huang, Junjie Jiang, Zinan Huang and Chengbo Mou * 

Key Laboratory of Specialty Fiber Optics and Optical Access Networks, Joint International Research Laboratory of Specialty Fiber Optics and Advanced Communication, Shanghai Institute for Advanced Communication and Data Science, Shanghai University, Shanghai 200444, China; li_kai@shu.edu.cn (K.L.);

huangqq@shu.edu.cn (Q.H.); jiangjunjie@shu.edu.cn (J.J.); zinanhuang@shu.edu.cn (Z.H.)

* Correspondence: mouc1@shu.edu.cn

Abstract: A wavelength-tunable high repetition rate (HRR) erbium-doped fiber laser in L-band based on dissipative four-wave mixing (DFWM) mechanism is demonstrated. The cavity can generate a single-soliton train and bound-soliton train with a fixed repetition rate of ~126 GHz, which is determined by the free spectral range of the intra-cavity Lyot filter. A wide wavelength-tuning operation can also be obtained by rotating the polarization controllers. The wavelength-tuning ranges of the HRR single-soliton state and HRR bound-soliton state are ~38.3 nm and ~22.6 nm, respectively. This laser provides useful references for the area of a wavelength-tunable fiber laser with high repetition rate. The laser may also find useful applications in high-speed communication, sensing, etc.



Citation: Li, K.; Huang, Q.; Jiang, J.; Huang, Z.; Mou, C. Wavelength-Tunable L-Band High Repetition Rate Erbium-Doped Fiber Laser Based on Dissipative Four-Wave Mixing. *Sensors* **2021**, *21*, 5975. <https://doi.org/10.3390/s21175975>

Academic Editors: Bernhard Wilhelm Roth, Limin Xiao, Sergio G. Leon-Saval and Tijmen G. Euser

Received: 28 July 2021

Accepted: 1 September 2021

Published: 6 September 2021

Publisher's Note: MDPI stays neutral with regard to jurisdictional claims in published maps and institutional affiliations.



Copyright: © 2021 by the authors. Licensee MDPI, Basel, Switzerland. This article is an open access article distributed under the terms and conditions of the Creative Commons Attribution (CC BY) license (<https://creativecommons.org/licenses/by/4.0/>).

Keywords: dissipative four-wave mixing; wavelength tunability; high repetition rate; erbium-doped fiber laser

1. Introduction

In recent decades, mode-locked fiber lasers with wavelength tunability have attracted great attention for various applications, such as micromachining, sensing, spectroscopy, and optical communication [1–3]. In particular, for high-speed optical communication systems, the conventional C-band (1530–1565 nm) is unable to meet the increasing requirement of communication capacity. Therefore, it is of great significance to investigate L-band (1565–1625 nm) wavelength-tunable mode-locked fiber lasers. Experimentally, there are two major ways to achieve wavelength tunability. The first is incorporating a tunable spectral filter in the cavity, such as a W-shaped long-period fiber grating (LPFG) filter [4], chirped fiber Bragg grating [5], birefringence-induced fiber filter [6], and commercial tunable band-pass filter [7]. The other method is to control intra-cavity loss by using some special elements, such as a tunable-ratio optical coupler [8], fiber taper [9], mechanical attenuator [10], and LPFG-based narrow-band optical attenuator [11]. However, these conventional wavelength-tunable EDFLs mostly operate at the repetition rate of megahertz. In order to make full use of the L-band for optical communication, it is also necessary to improve the repetition rate of the EDFLs to gigahertz (GHz).

To achieve a high-repetition rate (HRR) pulse train, a variety of passive mode-locking mechanisms have been reported, such as harmonic mode locking [12–14], short cavity [15,16], and dissipative four-wave mixing (DFWM) [17,18]. Compared to harmonic mode locking and short cavity, DFWM is a simpler and more effective method to generate an HRR pulse train with a capability even up to terahertz. In order to achieve a DFWM mode-locking operation, large nonlinearity is necessary, which contributes to phase matching between longitudinal modes in the cavity. Such intra-cavity nonlinearity can be enhanced by inserting a segment of highly nonlinear fiber, i.e., photonic crystal fiber [19]. In addition,

an intra-cavity comb filter is mandatory. Due to the unflatness of gain spectrum and limited gain bandwidth of gain fiber, a two-hump filtering configuration is formed by a combination of a comb filter and a segment of gain fiber. Therefore, under the joint function of this two-hump filtering effect and intra-cavity nonlinearity, only two modes selected by this two-hump filtering effect can experience net gain and transfer their energy into high-order harmonics unidirectionally, which are in the region of negative gain by a four-wave mixing effect. Then, an HRR pulse train is finally formed with a repetition rate defined by the free spectral range (FSR) of the comb filter. During the past decades, various schemes based on DFWM have been reported, such as sampled fiber Bragg grating [18,20–22], F-P filters [23,24], Mach–Zehnder interferometers [25,26], Lyot filters [27,28], programmable optical processors [29,30], and microring resonators [31,32]. In particular, J. Schröder et al. experimentally obtained up to a 20 nm wavelength tunability by incorporating a programmable optical processor in the cavity [29]. However, the large insertion loss and cost of the programmable optical processor make it impossible to be widely used. Through inserting an F-P filter, X. M. Tan et al. achieved a wavelength-tunable and switchable dual-waveband operation in an HRR EDFL, while the wavelength-tuning range was less than 15.2 nm [33]. Considering the importance of L-band and wavelength tunability, it is interesting to investigate a widely wavelength-tunable L-band HRR EDFL.

Herein, we experimentally demonstrate a widely wavelength-tunable L-band HRR EDFL for the first time. A pulse train with a repetition rate of ~126 GHz is obtained. In our laser, a fiber-based Lyot filter composed of a polarization dependent isolator (PD-ISO) and a piece of polarization-maintaining (PM) fiber is used to achieve a DFWM effect. Due to the existence of such a Lyot filter, the cavity can generate two kinds of HRR pulse trains. One is a single-soliton HRR pulse train with a wavelength-tuning range of ~38.3 nm (from 1569.83 nm to 1608.21 nm). The other status is an HRR bound-soliton pulse train, which can be achieved by rotating polarization controllers (PCs). In this state, the spectral center wavelength can be adjusted from 1578.98 nm to 1601.60 nm (~22.6 nm). Moreover, the conventional noise-like pulse (NLP) can also be observed when the intra-cavity polarization state is adjusted in some specific regime. We believe this fiber laser will provide an important reference for future research on wavelength-tunable HRR EDFLs.

2. Experimental Setup

The experimental setup of the fiber laser is shown schematically in Figure 1. The total cavity length is ~12.53 m, composed of a 2.59 m long erbium-doped fiber (EDF) (OFS Er80) with a group velocity dispersion (GVD) of +61.2 ps²/km as the gain medium, 1.23 m HI 1060 FLEX with a GVD of −7 ps²/km, 5.51 m PM fiber (YOFC, PM1550 125-13/250) with a GVD of −22.8 ps²/km, and ~3.20 m single mode fiber (SMF) with a GVD of −22.8 ps²/km. The net cavity dispersion is ~−0.048 ps². Two 980 nm laser diodes (LDs) provide a total maximum pump power of ~1.66 W (LD1, CM97-1050-76 with maximum power is ~1 W and LD2, YMPSS-980-660-B-FBG with maximum power is ~660 mW) from two directions, through two wavelength division multiplexers (WDM). A PD-ISO is inserted into the cavity to ensure the light is linearly polarized and to prevent bidirectional transmission. Two PCs are used to adjust intra-cavity polarization, and the 5:95 optical coupler (OC) outputs 5% laser energy.

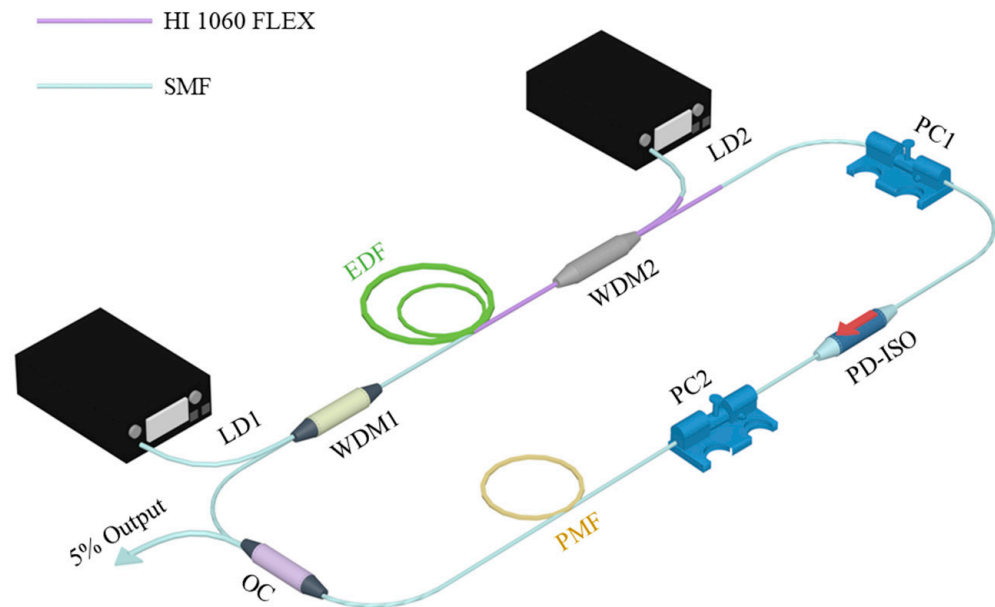


Figure 1. Experimental setup of HRR erbium-doped fiber laser.

Due to the existence of PD-ISO and PMF, a wavelength-dependent birefringence-induced filter with a comb transmission spectrum is formed in the cavity [34,35]. This filter is also called a Lyot filter and its transmission function can be described as [36,37]

$$T = \cos^2 \theta_1 \cos^2 \theta_2 + \sin^2 \theta_1 \sin^2 \theta_2 + \frac{1}{2} \sin(2\theta_1) \sin(2\theta_2) \cos(\Delta\varphi_L + \Delta\varphi_{NL}) \quad (1)$$

In Equation (1), θ_1 and θ_2 are azimuth angles of the two ends of the polarizer relative to the fast axis of the PMF. $\Delta\varphi_L = 2\pi L\Delta n/\lambda$ is the linear phase delay, and $\Delta\varphi_{NL} = 2\pi n_2 PL \cos(2\theta_1)/(\lambda A_{eff})$ is the nonlinear phase delay. L and Δn are length and birefringence intensity of PMF, respectively. λ is laser's operating wavelength, n_2 is nonlinear coefficient, P is instantaneous power of optical signal, and A_{eff} is effective area of core of PMF. Additionally, the FSR of fiber-based Lyot filter can be calculated by [27]

$$\Delta\lambda = \frac{\lambda^2}{L\Delta n} \quad (2)$$

The modal birefringence of PMF used in cavity is 4.32×10^{-4} . Since the transmission spectrum of the filter is only related to PMF, we disconnected the connection between the coupler and the PMF and spliced a polarizer after the PMF to measure the transmission spectrum of the fiber-based Lyot fiber. As shown in Figure 2a, the solid line is the experimental measurement result, and the FSR is ~ 126 GHz. The dashed line is the simulated result, which is in good agreement with the measured results. We also measured the transmission spectrum at different polarization states, which is illustrated in Figure 2b. The depth of the transmission spectrum changes with the adjustment of the orientations of PCs. We also simulated the transmission spectrum under different angles of θ_1 and θ_2 (dashed line in Figure 2(b-1,b-2)), which is in good agreement with the experimental results.

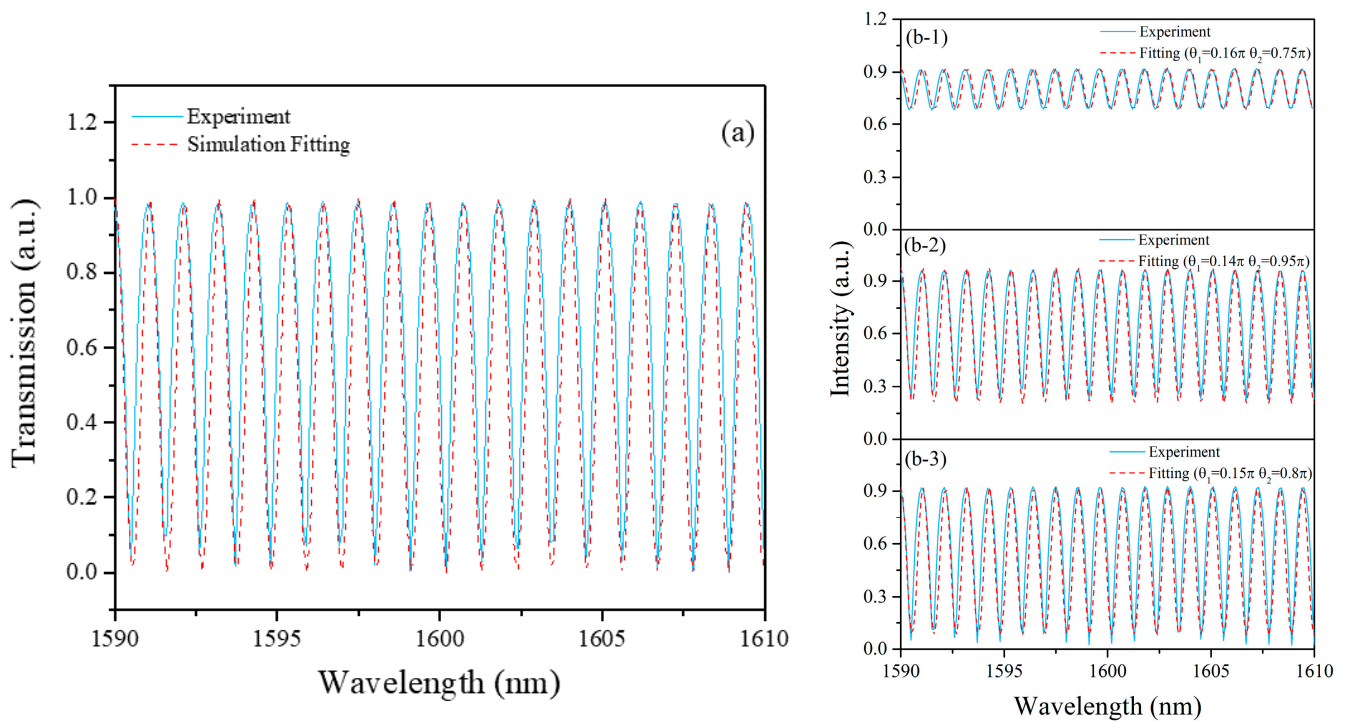


Figure 2. (a) Transmission spectrum of fiber-based Lyot filter in L-band (solid, experimental result; dashed, simulated result). (b-1–b-3) Transmission spectrum with different angles of θ_1 and θ_2 (solid, experimental result; dashed, simulated result).

3. Experimental Results and Discussions

3.1. HRR Output with the Repetition Rate of ~ 126 GHz

Due to the spectral filtering effect of the fiber-based Lyot filter, the DFWM mode-locking operation self-starts under the forward (LD1) and backward (LD2) pump power of 332 mW and 200 mW. Figure 3 shows a stable HRR single-soliton train when the pump power of LD1 and LD2 is 865 mW and 500 mW. The output power of the cavity is 13.69 mW. Figure 3a is the measured comb spectrum with a center wavelength of 1604.30 nm and a peak-to-peak interval of 1.08 nm, which corresponds to ~ 126 GHz. Here, we attribute this L-band oscillation to the in-band absorption of EDF [38,39]. The autocorrelation (AC) trace of the single-soliton train shown in Figure 3b has a pulse-to-pulse interval of 8.04 ps, which is in good agreement with the interval of spectral peaks. Additionally, the inset in Figure 3b is the measurement result across the entire scanning range. It is noted that the AC traces have a continuous wave background, and the pulse sequence is not flat. We speculate that this unflatness of the pulse intensity may be caused by the modulation instability of the two main spectral peaks [27].

When we keep the pump power of LD1 and LD2 fixed at 715 mW and 500 mW, the wavelength tuning operation can be achieved by carefully adjusting PCs. As illustrated in Figure 4a, the center wavelength of the HRR single-soliton train can be tuned from 1569.83 nm to 1608.21 nm, with a wavelength tuning range of ~ 38.3 nm in the L-band. To our best knowledge, this is the widest spectral-tuning range from which the DFWM fiber laser works in the L-band so far. During the process of wavelength tuning, the HRR single-soliton train has been well maintained, which is demonstrated in Figure 4b. We believe that such wavelength tunability is attributed to broad transmission characteristics of the intra-cavity Lyot filter in the L-band. The orientations of PCs lead to the change of modulation depth of the Lyot filter and the position of maximum gain, which shift the center wavelength of output pulses. In particular, this spectral tuning process is reversible.

Keeping the pump power fixed and further adjusting the orientations of PCs, the bound-soliton state can be obtained with the output power of 8.275 mW and the repetition rate of a unit of bound solitons also matches the frequency spacing of the Lyot filter. We believe that modulation instability has played a role in the formation of the HRR bound-

soliton train, altering the repetition unit of the cavity emission [27]. The measured results are shown in Figure 5. The middle of the spectrum is concave, and the peaks on two sides are the strongest in Figure 5a, which is a typical characteristic of the bound-soliton state. The peak-to-peak interval of the spectrum is 1.06 nm, corresponding to a repetition rate of ~ 126 GHz. Figure 5b shows the AC traces with an interval of ~ 8.03 ps, which is consistent with the result in the HRR single-soliton state. In addition, it seems that the pulse-to-pulse interval in a single bound soliton is related to the spectrum. The interval between two highest peaks is 3.18 nm, corresponding to a repetition rate of ~ 380 GHz, which matches well with the side-pulse interval of 2.62 ps.

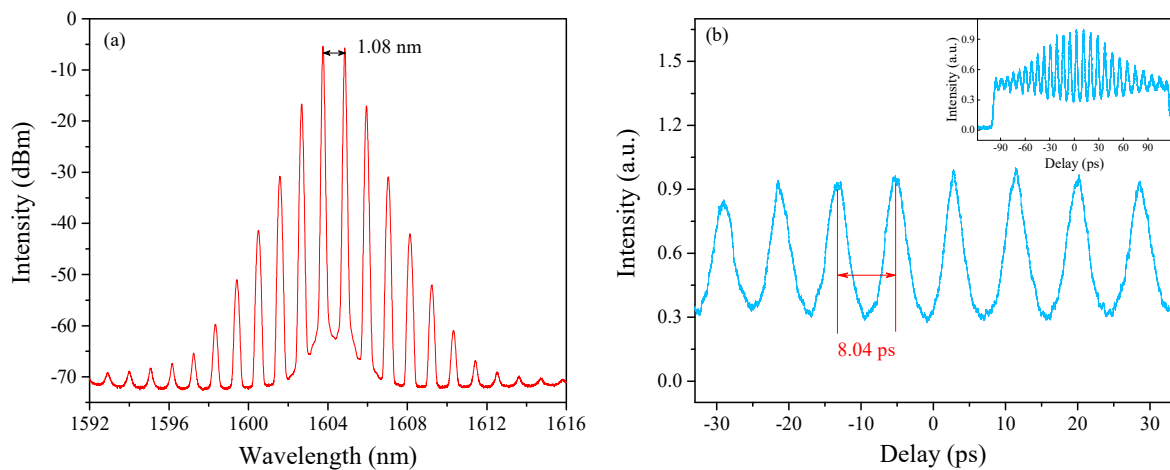


Figure 3. Output characteristics of laser cavity based on Lyot filter-driven DFWM. (a) Optical spectrum. (b) AC traces; the inset figure is the full scanning measured result.

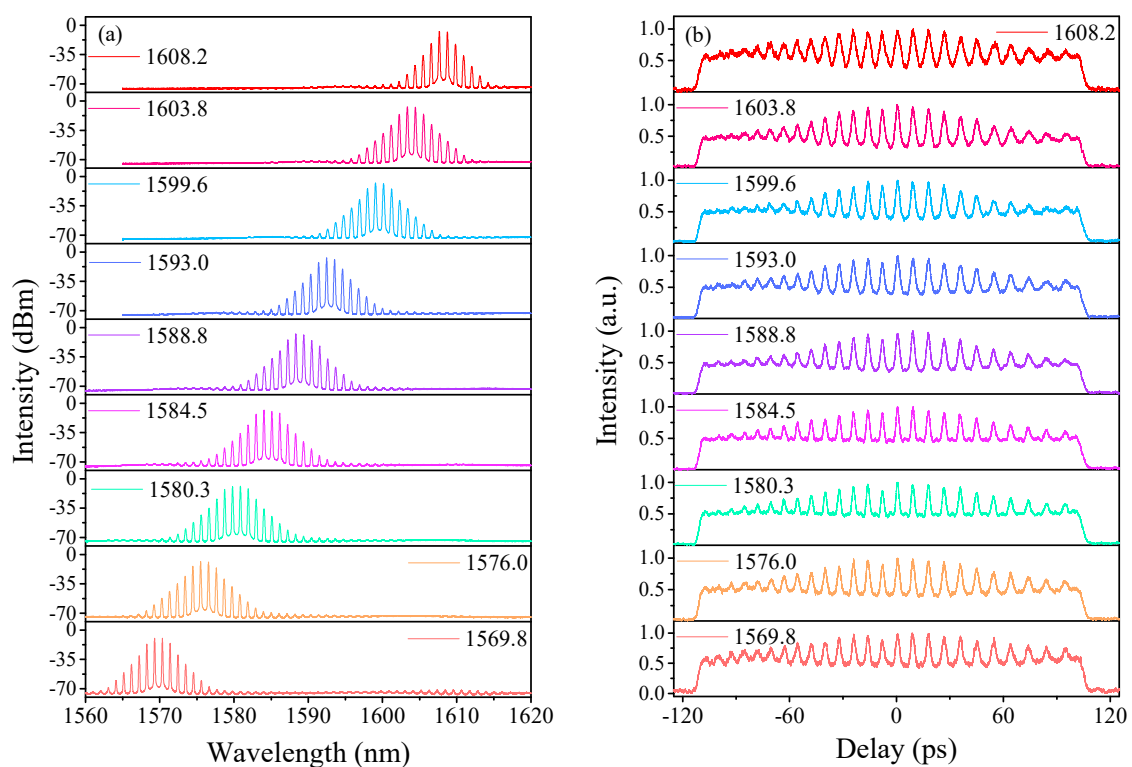


Figure 4. HRR single-soliton train for various orientations of PCs. (a) Optical spectra at various central wavelengths. (b) Corresponding AC traces.

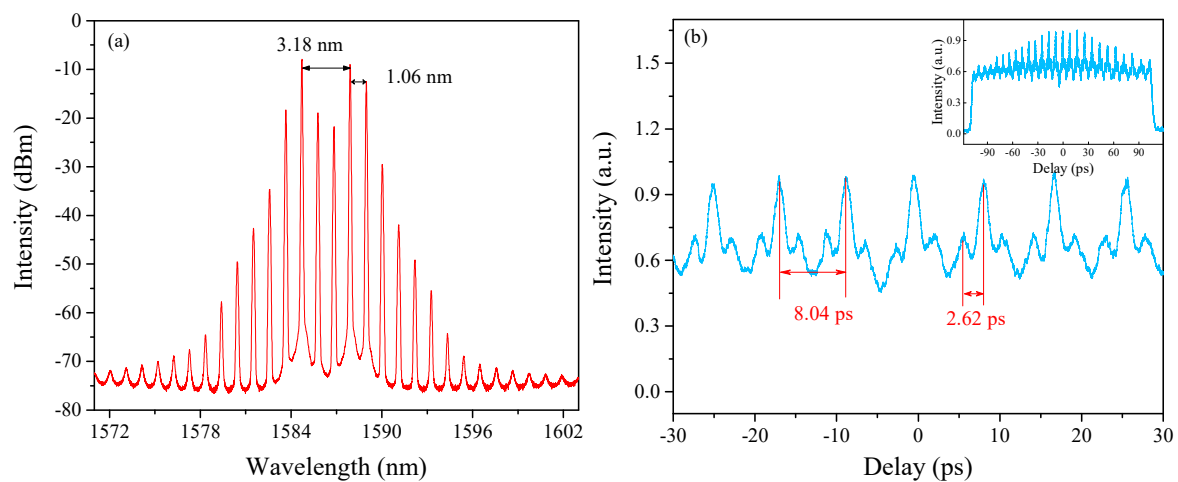


Figure 5. HRR Bound-soliton train. (a) Optical spectrum. (b) AC traces; the inset figure is full span measurement.

Similar to the situation of the HRR single-soliton state, the center wavelength of the spectrum in the bound-soliton state is also tunable. As illustrated in Figure 6a, the center wavelength has been shifted from 1578.98 nm to 1601.60 nm through adjusting PCs carefully and slowly, with a wavelength tuning range of ~ 22.6 nm in the L-band. Figure 6b exhibits the corresponding AC traces of the HRR bound-soliton state. There always is a strong background pedestal in measured AC traces regardless of HRR single-soliton or HRR bound-soliton emissions. This phenomenon may be caused by supermode noise in the cavity [20,26] and can be suppressed by inserting a sub-cavity structure for enhanced filtering [26] or using a high-finesse filter instead [40–42].

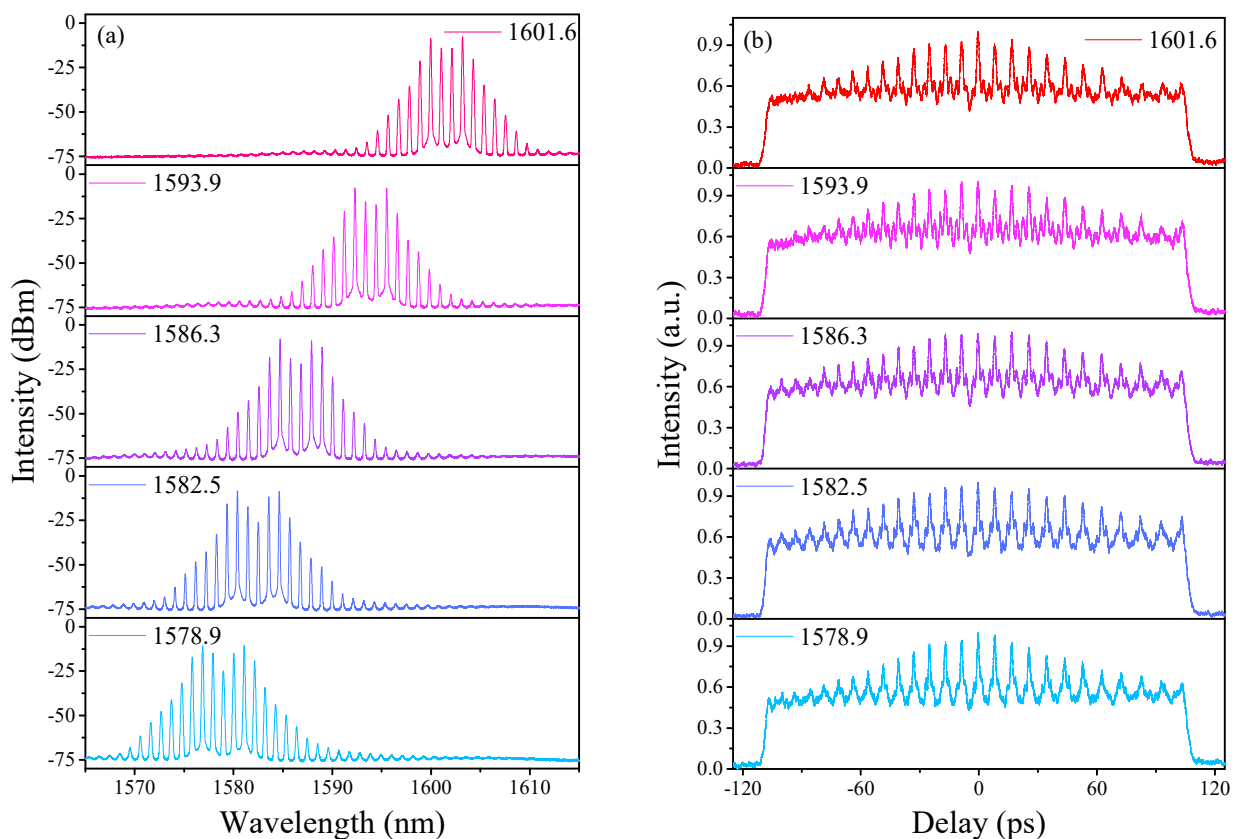


Figure 6. HRR bound-soliton train for different polarization states. (a) Optical spectra at various central wavelengths. (b) Corresponding AC traces.

3.2. HRR Output with the Repetition Rate of ~ 71 GHz

In our experiment, HRR EDFLs with different repetition rates can be obtained by merely changing the length of PMF. This is because the FSR of the fiber-based Lyot filter is related to the length of PMF. For example, if we want to achieve a pulse train with a repetition rate of ~ 70 GHz in the L-band, the calculated length of PMF is 10 m, and the corresponding FSR is ~ 0.6 nm. In order to verify this, we insert a 10 m PMF into the cavity. When the pump power of LD1 and LD2 is 893 mW and 660 mW, the HRR single-soliton train can be generated. Figure 7a shows the corresponding optical spectrum with a peak-to-peak interval of 0.61 nm, which is consistent with the calculated result. Additionally, the interval of pulses is measured to be ~ 14.39 ps. The experimental results strongly prove the efficiency of this technique. Keeping the pump power fixed, the above-mentioned wavelength-tuning operation can be obtained by adjusting PCs. As exhibited in Figure 8a, the central wavelength of the spectrum has been tuned from 1572.58 nm to 1608.12 nm, nearly 35.6 nm. Additionally, the corresponding AC traces are shown in Figure 8b. In addition, the HRR bound-soliton trains with the same repetition rate of ~ 71 GHz and the corresponding wavelength-tuning operation can also be achieved, which are similar to the results in Figures 5 and 6.

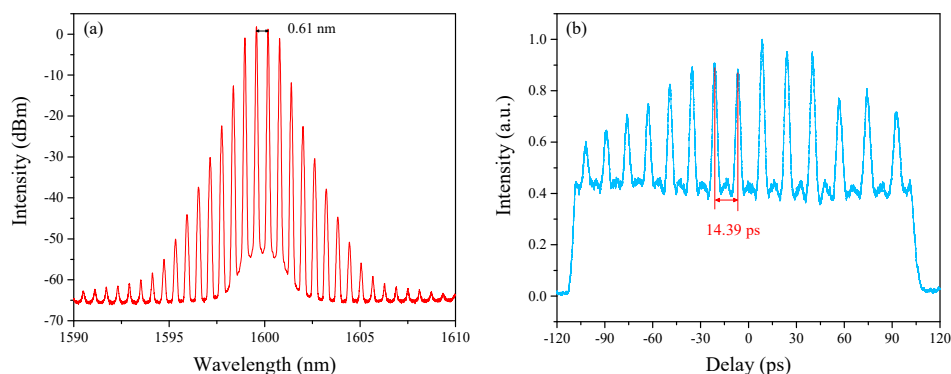


Figure 7. HRR single-soliton train when the length of intra-cavity PMF is 10 m. (a) Optical spectrum. (b) Corresponding AC traces.

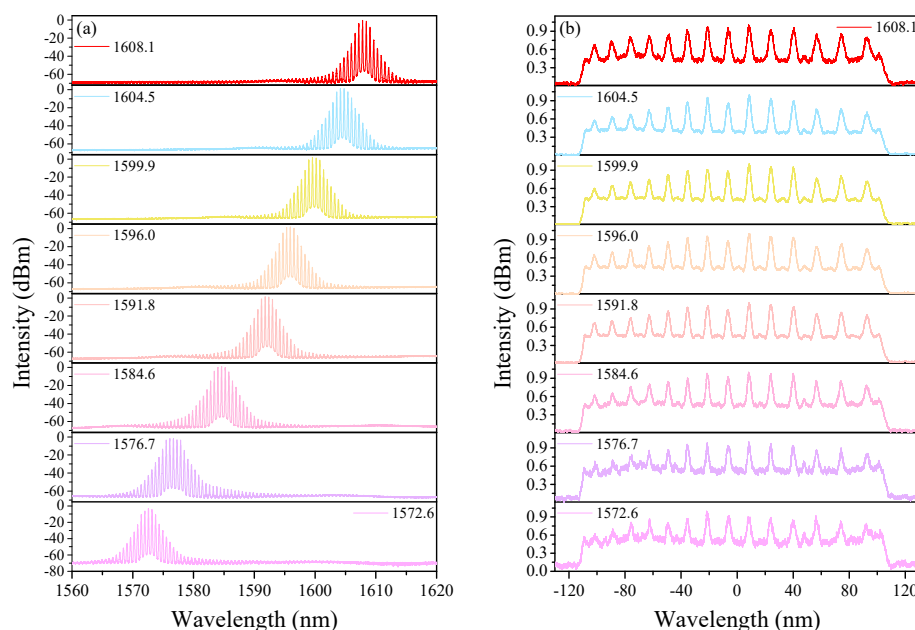


Figure 8. HRR single-soliton train for different polarization states when the length of intra-cavity PMF is 10 m. (a) Optical spectra at various central wavelengths. (b) Corresponding AC traces.

3.3. Noise-like Pulse Generation

In addition to the above-mentioned HRR pulse train emission, we can also observe NLP in this laser regardless of whether the length of the intra-cavity PMF is 5.51 m or 10 m. When the orientations of PCs were adjusted to make the transmission coefficient very small, the comb filtering characteristic of the Lyot filter was suppressed. Therefore, the DFWM effect became weak and could not support the formation of the HRR pulse train, finally resulting in the generation of NLP. For example, when the length of PMF is 5.51 m, it is observed that the NLP is generated by adjusting PCs carefully under the total pump power of 1.215 W. The measurement results are shown in Figure 9. The center wavelength and full width at half height (FWHM) of the optical spectrum are 1607.07 nm and 28.34 nm in Figure 9a. Figure 9b exhibits a typical AC trace of the NLP, which is composed of a broad pedestal and a narrow spike. Additionally, the FWHM of this narrow spike is 151 fs (sech² assumed). The corresponding pulse train shown in Figure 9c is measured by the oscilloscope connecting with a high-speed photo-detector (Newport 818-BB-51F, 12.5 GHz). The pulse interval is 61.51 ns, which matches well with the cavity length. As presented in Figure 9d, the signal noise ratio (SNR) is 37.8 dB. Additionally, the RF spectrum with a 3.2 GHz span is shown in the illustration.

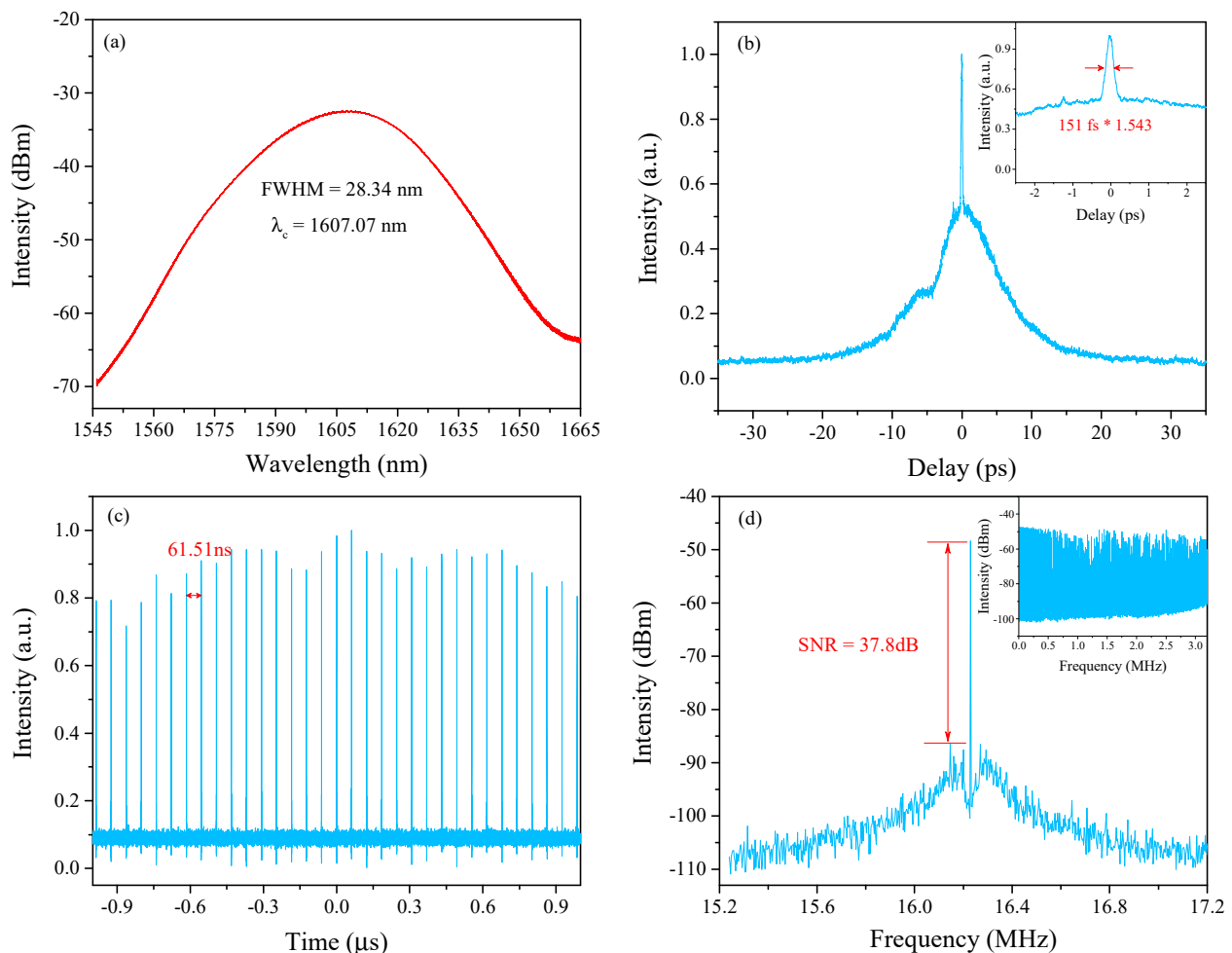


Figure 9. Measurement results of NLP. (a) Optical spectrum. (b) AC trace; the inset figure is the narrow spike. (c) Pulse train measured by oscilloscope. (d) RF spectrum with a span and resolution of 2 MHz and 300 Hz; the inset figure is the RF spectrum with a span and resolution of 3.2 GHz and 10 kHz.

3.4. Stability Measurements

We also perform an experiment to verify the stability of this laser when the PMF is 5.51 m. Increasing the pump power of LD1 and LD2 to 893 mW and 660 mW and ensuring the cavity is working in an HRR single-soliton operation, the laser output is repeatedly recorded at an interval of 5 min for 45 min. As exhibited in Figure 10, the central wavelength drift and intensity fluctuation are 0.19 nm and 0.14 mW, respectively, indicating the good stability of this HRR EDFL.

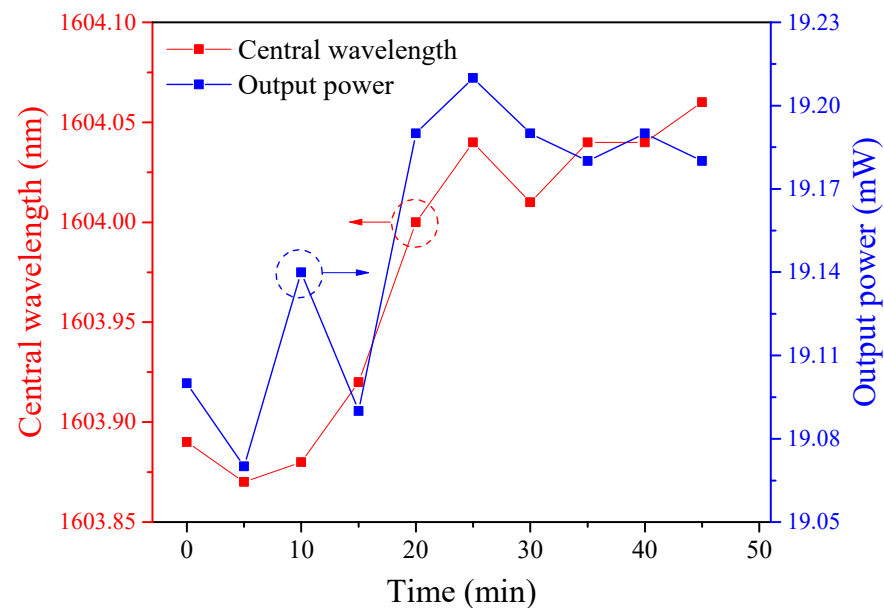


Figure 10. Stability measurements of central wavelength and output power for 45 min when the length of PMF is 5.51 m.

4. Conclusions

In conclusion, we experimentally demonstrate a wide wavelength-tunable L-band HRR EDFL based on a DFWM mode-locking mechanism. Due to the existence of an intra-cavity fiber-based Lyot filter, the repetition rate of the pulse train is fixed at ~ 126 GHz. Under the forward and backward pump power of 715 mW and 500 mW, two kinds of HRR pulse sequences, i.e., HRR single-soliton train and HRR bound-soliton train, can be obtained. With the broad transmission spectrum of this comb filter, the wavelength-tuning operation has been achieved by rotating the PCs in both pulse regimes. The center wavelength-tuning range in the HRR single-soliton state and HRR bound-soliton state is ~ 38.3 nm and ~ 22.6 nm, respectively. Compared to other filters, this technique especially has better flexibility. On the one hand, this fiber-based filter allows for an all-fiber structure, which has higher compactness and lower insertion loss. On the other hand, due to the FSR of this fiber-based Lyot filter being related to the length of PMF in the cavity, we can select the appropriate length to obtain a pulse train with the required repetition rate for different applications. Our research provides an easy and effective method to achieve a wavelength-tunable GHz HRR EDFL in the L-band, which will contribute to the development of wavelength-tunable HRR EDFLs. In addition, such high-repetition-rate comb fiber lasers can also work as seed sources for sensing, such as coherent ranging [43], gas detection at 1.5–1.6 μm [44], and temperature sensing [45].

Author Contributions: C.M. conceived the idea and supervised the project; K.L. carried out the experiment and data analysis; J.J. carried out the data processing; Q.H., Z.H. and other authors were involved in the writing and discussion. All authors have read and agreed to the published version of the manuscript.

Funding: This research was funded by the National Science Foundation of China (61975107, 62135007, 61605107), the National key research and development program of China (2020YFB1805800), the Natural Science Foundation of Shanghai (20ZR1471500), and the “111” project (D20031).

Institutional Review Board Statement: Not applicable.

Informed Consent Statement: Not applicable.

Data Availability Statement: Not applicable.

Conflicts of Interest: The authors declare no conflict of interest.

References

1. Chen, N.-K.; Lin, J.-W.; Liu, F.-Z.; Liaw, S.-K. Wavelength-Tunable Er³⁺-Doped fs Mode-Locked Fiber Laser Using Short-Pass Edge Filters. *IEEE Photonics Technol. Lett.* **2010**, *22*, 700–702. [[CrossRef](#)]
2. Fermann, M.E.; Hartl, I. Ultrafast fibre lasers. *Nat. Photonics* **2013**, *7*, 868–874. [[CrossRef](#)]
3. Brida, D.; Krauss, G.; Sell, A.; Leitenstorfer, A. Ultrabroadband Er: fiber lasers. *Laser Photonics Rev.* **2014**, *8*, 409–428. [[CrossRef](#)]
4. Wang, J.; Zhang, A.P.; Shen, Y.H.; Tam, H.Y.; Wai, P.K. Widely tunable mode-locked fiber laser using carbon nanotube and LPG W-shaped filter. *Opt. Lett.* **2015**, *40*, 4329–4332. [[CrossRef](#)] [[PubMed](#)]
5. Yan, Y.; Wang, J.; Wang, L.; Cheng, Z. Wavelength tunable L Band polarization-locked vector soliton fiber laser based on SWCNT-SA and CFBG. *Opt. Commun.* **2018**, *412*, 55–59. [[CrossRef](#)]
6. Huang, Q.; Zou, C.; Mou, C.; Guo, X.; Yan, Z.; Zhou, K.; Zhang, L. 23 MHz widely wavelength-tunable L-band dissipative soliton from an all-fiber Er-doped laser. *Opt. Express* **2019**, *27*, 20028–20036. [[CrossRef](#)]
7. Zhang, Y. C + L band wavelength and bandwidth tunable fiber laser incorporating carbon nanotubes. *Mod. Phys. Lett. B* **2020**, *34*, 2050340. [[CrossRef](#)]
8. Lin, G.-R.; Chang, J.-Y. Femtosecond mode-locked Erbium-doped fiber ring laser with intra-cavity loss controlled full L-band wavelength tunability. *Opt. Express* **2007**, *15*, 97–103. [[CrossRef](#)]
9. Melo, M.; Frazão, O.; Teixeira, A.L.J.; Gomes, L.A.; da Rocha, J.R.F.; Salgado, H.M. Tunable L-band erbium-doped fibre ring laser by means of induced cavity loss using a fibre taper. *Appl. Phys. B* **2003**, *77*, 139–142. [[CrossRef](#)]
10. Zhu, T.; Wang, Z.; Wang, D.N.; Yang, F.; Li, L. Generation of wavelength-tunable and coherent dual-wavelength solitons in the C + L band by controlling the intracavity loss. *Photonics Res.* **2019**, *7*, 853–861. [[CrossRef](#)]
11. Jiang, J.; Huang, Q.; Ma, Y.; Liao, D.; Huang, Z.; Dai, L.; Liu, Y.; Mou, C.; Al Araimi, M.; Rozhin, A. Wavelength-tunable L-band mode-locked fiber laser using a long-period fiber grating. *Opt. Express* **2021**, *29*, 26332–26339. [[CrossRef](#)]
12. Ling, Y.; Huang, Q.; Zou, C.; Xing, Z.; Yan, Z.; Zhao, C.; Zhou, K.; Zhang, L.; Mou, C. L-Band GHz Femtosecond Passively Harmonic Mode-Locked Er-Doped Fiber Laser Based on Nonlinear Polarization Rotation. *IEEE Photonics J.* **2019**, *11*, 1–7. [[CrossRef](#)]
13. Huang, Q.; Huang, Z.; Al Araimi, M.; Rozhin, A.; Mou, C. 2.4 GHz L-Band Passively Harmonic Mode Locked Er-Doped Fiber Laser Based on Carbon Nanotubes Film. *IEEE Photonics Technol. Lett.* **2020**, *32*, 121–124. [[CrossRef](#)]
14. Ling, Y.; Huang, Q.; Song, Q.; Yan, Z.; Mou, C.; Zhou, K.; Zhang, L. Intracavity birefringence-controlled GHz-tuning range passively harmonic mode-locked fiber laser based on NPR. *Appl. Opt.* **2020**, *59*, 6724–6728. [[CrossRef](#)]
15. Du, W.; Xia, H.; Li, H.; Liu, C.; Wang, P.; Liu, Y. High-repetition-rate all-fiber femtosecond laser with an optical integrated component. *Appl. Opt.* **2017**, *56*, 2504–2509. [[CrossRef](#)]
16. Gao, X.; Zhao, Z.; Cong, Z.; Gao, G.; Zhang, A.; Guo, H.; Yao, G.; Liu, Z. Stable 5-GHz fundamental repetition rate passively SESAM mode-locked Er-doped silica fiber lasers. *Opt. Express* **2021**, *29*, 9021–9029. [[CrossRef](#)] [[PubMed](#)]
17. Quiroga-Teixeiro, M. Passive mode locking by dissipative four-wave mixing. *J. Opt. Soc. Am. B* **1998**, *15*, 1315–1321. [[CrossRef](#)]
18. Sylvestre, T.; Coen, S.; Emplit, P.; Haelterman, M. Self-induced modulational instability laser revisited: Normal dispersion and dark-pulse train generation. *Opt. Lett.* **2002**, *27*, 482–484. [[CrossRef](#)] [[PubMed](#)]
19. Yu, R.; Wang, C.; Benabid, F.; Chiang, K.S.; Xiao, L. Robust Mode Matching between Structurally Dissimilar Optical Fiber Waveguides. *ACS Photonics* **2021**, *8*, 857–863. [[CrossRef](#)]
20. Schröder, J.; Coen, S.; Vanholsbeeck, F.; Sylvestre, T. Dynamics of an ultrahigh-repetition-rate of a passively mode locked raman fiber laser. *J. Opt. Soc. Am. B* **2008**, *25*, 1178–1186. [[CrossRef](#)]
21. Schröder, J.; Coen, S.; Vanholsbeeck, F. Passively mode-locked Raman fiber laser with 100 GHz repetition rate. *Opt. Lett.* **2006**, *31*, 3489–3491. [[CrossRef](#)] [[PubMed](#)]
22. Zhang, S. Passive mode locking at harmonics of the free spectral range of the intracavity filter in a fiber ring laser. *Opt. Lett.* **2005**, *30*, 2852–2854. [[CrossRef](#)]
23. Yoshida, E.; Nakazawa, M. Low-threshold 115-GHz continuous-wave modulational-instability erbium-doped fiber laser. *Opt. Lett.* **1997**, *22*, 1409–1411. [[CrossRef](#)] [[PubMed](#)]
24. Qi, Y.L.; Liu, H.; Cui, H.; Huang, Y.Q.; Ning, Q.Y.; Liu, M.; Luo, Z.C.; Luo, A.P.; Xu, W.C. Graphene-deposited microfiber photonic device for ultrahigh-repetition rate pulse generation in a fiber laser. *Opt. Express* **2015**, *23*, 17720–17726. [[CrossRef](#)]
25. Mao, D.; Liu, X.; Sun, Z.; Lu, H.; Han, D.; Wang, G.; Wang, F. Flexible high-repetition-rate ultrafast fiber laser. *Sci. Rep.* **2013**, *3*, 1–5. [[CrossRef](#)]

26. Si Fodil, R.; Amrani, F.; Yang, C.; Kellou, A.; Grelu, P. Adjustable high-repetition-rate pulse trains in a passively-mode-locked fiber laser. *Phys. Rev. A* **2016**, *94*, 013813. [[CrossRef](#)]
27. Zhao, L.M.; Tang, D.Y.; Liu, D. Ultrahigh-repetition-rate bound-soliton fiber laser. *Appl. Phys. B* **2010**, *99*, 441–447. [[CrossRef](#)]
28. Zadok, A.; Sendowski, J.; Yariv, A. Birefringence-Induced Trains of High-Rate Pulses in a Mode-Locked Fiber Laser. *IEEE Photonics J.* **2009**, *1*, 128–134. [[CrossRef](#)]
29. Schröder, J.; Vo, T.D.; Eggleton, B.J. Repetition-rate-selective, wavelength-tunable mode-locked laser at up to 640 GHz. *Opt. Lett.* **2009**, *34*, 3902–3904. [[CrossRef](#)]
30. Schröder, J.; Coen, S.; Sylvestre, T.; Eggleton, B.J. Dark and bright pulse passive mode-locked laser with in-cavity pulse-shaper. *Opt. Express* **2010**, *18*, 22715–22721. [[CrossRef](#)]
31. Peccianti, M.; Pasquazi, A.; Park, Y.; Little, B.E.; Chu, S.T.; Moss, D.J.; Morandotti, R. Demonstration of a stable ultrafast laser based on a nonlinear microcavity. *Nat. Commun.* **2012**, *3*, 1–6. [[CrossRef](#)]
32. Liu, M.; Tang, R.; Luo, A.-P.; Xu, W.-C.; Luo, Z.-C. Graphene-decorated microfiber knot as a broadband resonator for ultrahigh-repetition-rate pulse fiber lasers. *Photonics Res.* **2018**, *6*, C1–C7. [[CrossRef](#)]
33. Tan, X.M.; Chen, H.J.; Cui, H.; Lv, Y.K.; Zhao, G.K.; Luo, Z.C.; Luo, A.P.; Xu, W.C. Tunable and switchable dual-waveband ultrafast fiber laser with 100 GHz repetition-rate. *Opt. Express* **2017**, *25*, 16291–16299. [[CrossRef](#)]
34. Liu, S.; Yan, F.; Ting, F.; Zhang, L.; Bai, Z.; Han, W.; Zhou, H. Multi-Wavelength Thulium-Doped Fiber Laser Using a Fiber-Based Lyot Filter. *IEEE Photonics Technol. Lett.* **2016**, *28*, 864–867. [[CrossRef](#)]
35. Luo, Z.C.; Luo, A.P.; Xu, W.C.; Yin, H.S.; Liu, J.R.; Ye, Q.; Fang, Z.J. Tunable Multiwavelength Passively Mode-Locked Fiber Ring Laser Using Intracavity Birefringence-Induced Comb Filter. *IEEE Photonics J.* **2010**, *2*, 571–577.
36. Tang, D.Y.; Zhao, L.M.; Zhao, B.; Liu, A.Q. Mechanism of multisoliton formation and soliton energy quantization in passively mode-locked fiber lasers. *Phys. Rev. A* **2005**, *72*, 043816. [[CrossRef](#)]
37. Chen, C.-J.; Wai, P.K.A.; Menyuk, C.R. Soliton fiber ring laser. *Opt. Lett.* **1992**, *17*, 417–419. [[CrossRef](#)]
38. Luo, J.L.; Li, L.; Ge, Y.Q.; Jin, X.X.; Tang, D.Y.; Shen, D.Y.; Zhang, S.M.; Zhao, L.M. L-Band Femtosecond Fiber Laser Mode Locked by Nonlinear Polarization Rotation. *IEEE Photonics Technol. Lett.* **2014**, *26*, 2438–2441. [[CrossRef](#)]
39. Kwon, W.S.; Lee, H.; Kim, J.H.; Choi, J.; Kim, K.-S.; Kim, S. Ultrashort stretched-pulse L-band laser using carbon-nanotube saturable absorber. *Opt. Express* **2015**, *23*, 7779–7785. [[CrossRef](#)] [[PubMed](#)]
40. Pasquazi, A.; Peccianti, M.; Park, Y.; Little, B.E.; Chu, S.T.; Moss, D.J.; Morandotti, R. Highly Stable 200 GHz Soliton Microring Resonator Laser based on Filter-Driven Four Wave Mixing. In Proceedings of the CLEO: Applications and Technology, Baltimore, MD, USA, 1–6 May 2011; p. JWA10.
41. Yilmaz, S.; Sayinc, H.; Ilday, F.Ö.; Neumann, J.; Kracht, D. Intracavity Dissipative Four-Wave Mixing at Different Dispersion Regimes of an Ultrafast Fiber Laser. In Proceedings of the Frontiers in Optics, Rochester, NY, USA, 17–21 October 2016; p. FTu11.4.
42. Bao, H.; Cooper, A.; Chu, S.T.; Moss, D.J.; Morandotti, R.; Little, B.E.; Peccianti, M.; Pasquazi, A. Type-II micro-comb generation in a filter-driven four wave mixing laser. *Photon. Res.* **2018**, *6*, B67–B73. [[CrossRef](#)]
43. Riemensberger, J.; Lukashchuk, A.; Karpov, M.; Weng, W.L.; Lucas, E.; Liu, J.Q.; Kippenberg, T.J. Massively parallel coherent laser ranging using a soliton microcomb. *Nature* **2020**, *70*, 164–170. [[CrossRef](#)] [[PubMed](#)]
44. Rutkowski, L.; Johansson, A.C.; Valiev, D.; Khodabakhsh, A.; Tkacz, A.; Schmidt, F.M.; Foltynowicz, A. Detection of OH in an atmospheric flame at 1.5 μm using optical frequency comb spectroscopy. *Photonics Lett. Pol.* **2016**, *8*, 110–112. [[CrossRef](#)]
45. Cai, X.; Luo, J.; Fu, H.; Bu, Y.; Chen, N. Temperature measurement using a multi-wavelength fiber ring laser based on a hybrid gain medium and Sagnac interferometer. *Opt. Express* **2020**, *28*, 39933–39943. [[CrossRef](#)]